NMR study of the metal-insulator transition in the compensated sodium-tungsten bronze, $Na_xTa_yW_{1-y}O_3$

M. A. Dubson* and D. F. Holcomb
Laboratory of Atomic and Solid State Physics, Cornell University, Ithaca, New York 14853-2501
(Received 10 January 1986)

The NMR properties of the ^{183}W spin system have been measured in the nonstoichiometric compound $Na_xTa_yW_{1-y}O_3$, $0<x,y<1$. This material, called a bronze, undergoes a metal-insulator (M-I) transition at $x-y=0.18$ while maintaining a cubic-crystal phase. The ^{183}W NMR properties measured include the Knight shift, the line shape, the spin-lattice relaxation time T_1, and the spin-spin phase memory time T_2. The measurements were made in a field of 6.0 T at temperatures of 4.2 and 77 K. As the sample composition is varied from metallic to insulating, the recovery curves of the W nuclear magnetization at 4.2 K evolve smoothly from an exponential curve with a T_1 of a few seconds to a dramatically nonexponential curve with a distribution of relaxation times ranging from seconds to days. The combination of the small moment of ^{183}W and wide, inhomogeneously broadened NMR lines inhibits spin diffusion so that spins relax at a rate determined by their immediate electronic environments. The distribution of T_1's thus probes the distribution of local electronic environments in this disordered material.

I. INTRODUCTION

The nonstoichiometric compound Na_xWO_3 ($0<x<1$), often called a tungsten bronze, undergoes a transition from semiconducting to metallic behavior as x is increased through a critical x value of about 0.17 (Refs. 1 and 2). On the metal side of the transition ($x>0.2$), a cubic perovskite crystal structure is stable, but as x is lowered below 0.2, a series of structural phase transitions occurs, obscuring the metal-insulator (M-I) transition.[3,4]

Although details of the M-I transition remain obscure, a fairly complete picture of the physics of cubic, metallic Na_xWO_3 has emerged over the years.[5] The conduction band is made up of tungsten $5d$ and oxygen $2p$ orbitals. Sodium atoms act as donors of conduction electrons, with each sodium contributing one electron to the conduction band but not drastically altering the wave-function character of the band. The exact extent to which the sodium atoms change the conduction-band shape (i.e., whether a rigid-band model has any validity) is a subject of controversy. In any case, the band picture must be incomplete in the vicinity of the transition. A band model can predict a M-I transition only by emptying a band. Consequently, any band model incorrectly predicts that the transition occurs at $x=0$.

In 1978, Doumerc and co-workers[6,7] discovered that the tantalum-doped bronze $Na_xTa_yW_{1-y}O_3$ also undergoes a M-I transition but maintains a cubic phase on both sides of the transition. The transition occurs when the composition parameter $x-y$ is about 0.2. Doumerc proposed that, on the metal side of the transition, the conduction-electron concentration goes as $x-y$. In Doumerc's view, sodium atoms act as donors, as in metallic Na_xWO_3, and tantalum atoms act as acceptors. His argument is simple. Tantalum is one place to the left of tungsten in the Periodic Table; it has one less electron. So when Ta substitutes for W, it must accept an electron from the conduction band in order to complete the covalent bonds with its oxygen nearest neighbors. Although there exists compelling qualitative evidence for Doumerc's $x-y$ model of simple compensation,[8] there exists no direct confirmation, such as Hall-coefficient measurements.

Here we report the results of a nuclear-magnetic-resonance (NMR) study of the M-I transition in cubic $Na_xTa_yW_{1-y}O_3$. We have prepared a series of clean, homogeneous samples which span the M-I transition and have measured the following ^{183}W NMR properties: Knight shift, line shape, spin-lattice relaxation time T_1, and spin-spin phase memory time T_2.

Most experimental probes of M-I transitions, such as transport property and tunneling conductance measurements, provide information on some global property of the system under study. In contrast, NMR experiments provide a local probe of the electronic structure. The NMR properties of Na_xWO_3 have been studied by several groups.[9-14,4] However, because the cubic phase of this material is stable only in metallic samples, no one has been able to follow its NMR properties through the transition. In the tantalum-doped bronze $Na_xTa_yW_{1-y}O_3$, we have a system which can be studied on both sides of the transition, allowing us to correlate changes in the conductivity, a global property, with changes in those features of the local electronic structure which are revealed by NMR.

Doped semiconductors, such as Si:P, represent similar but more intensively studied systems. An important difference between the classic impurity systems in Si and Ge and the bronzes is the relative impurity concentration at which the M-I transition occurs. The large Bohr radius of shallow impurities in Ge and Si leads to critical donor concentrations of 10^{17}–10^{19} cm^{-3}. For Na_xWO_3, the critical sodium content, $x=0.2$, corresponds to a donor concentration of 4×10^{21} cm^{-3}. For the bronzes, effects associated with the atomic granularity of the lattice are surely important, whereas for Ge and Si the ra-

dius of the bound-state impurity wave function is much larger than a host crystal lattice constant, leading to a picture of impurity atoms randomly occupying positions in a continuum. Comparison of the properties of these rather different materials, doped semiconductors and the bronzes, may help determine which features of the *M-I* transition are universal and which are system dependent.

II. SAMPLE PREPARATION AND ANALYSIS

The samples are prepared in two stages in a procedure which adds refinements to those of several previous workers.[15–17] First, by the process of fused-salt electrolysis, we grow large single crystals about a centimeter on an edge. The starting materials in the electrolytic growth are sodium tungstate, Na_2WO_4, tungsten trioxide, WO_3, and tantalum oxide, Ta_2O_5. In this way, we can make metallic samples with compositions in the range $0.55 < x < 0.85$, $0 < y < 0.18$. Then, to make weakly conducting and insulating samples, we must shatter the electrolytically grown single crystals and diffuse some of the sodium out of resulting debris by a process that involves baking at high temperatures. The final product is a chemically uniform powder with particle size of 30–100 μm. The same batch which produces a powder sample for NMR measurements also produces a few small single-crystal chips of nearly the same composition. These chips, with dimensions of less than a millimeter, are used for conductivity measurements. The samples are quite homogeneous with variations in sodium content x less than 0.002 and variations in tantalum content y of about 0.005.

Samples are analyzed by a combination of electron-probe microanalysis (EPMA) and precise lattice-constant measurements. Brown and Banks[18] discovered a linear relation between the lattice constant and the sodium content x in Na_xWO_3. This relation allows one to determine x from Debye-Scherrer x-ray powder patterns. Samples of Na_xWO_3 with x determined from lattice-constant measurements are then used as sodium standards in EPMA analysis of tantalum-doped samples. Because tungsten and tantalum are adjacent in the Periodic Table, W can be used as an internal standard for the analysis of Ta in $Na_xTa_yW_{1-y}O_3$. With this procedure, we can determine x and y with absolute accuracies of ± 0.01 and ± 0.005, respectively.

The issue of sample homogeneity is central to any experimental study of the electronic structure of disordered systems. If the scale of inhomogeneity is large, say, micrometers, as in a percolating network of micrometer-sized metallic particles in a dielectric medium, then classical percolation is a valid model. If the inhomogeneity is truly microscopic, as in a doped semiconductor, then quantum effects are dominant, and one must seek quantum models: Anderson localization, interaction effects, etc. We believe that the samples of $Na_xTa_yW_{1-y}O_3$ studied here are systems with truly microscopic disorder; that is, the sodium and tantalum atoms are distributed among the available sites in the atomic lattice at random. The evidence for homogeneity comes from the appearance of polished surfaces, EPMA scans, x-ray linewidths, and NMR absorption line shapes. We discuss the first three of these clues here. Discussion of the significance of the NMR line shapes is given in Sec. VI.

The color of the bronzes varies dramatically with composition. As the parameter $x-y$ varies from 0.9 to 0.1 in $Na_xTa_yW_{1-y}O_3$, the color changes from a yellow-green for 0.9 to gold for 0.75, red for 0.6, purple for 0.5, blue for 0.4, dark royal blue for 0.3, and a blue-black below 0.2. Small variations in the color of a smooth, polished surface indicate composition variations. EPMA scans of inhomogeneous samples show that variations in x or y as small as 0.01 are easily seen as color variations on flat surfaces. The uniform color of our samples indicates that they are homogeneous on the scale of visible light, namely, 1 μm.

In those samples which undergo a sodium-dilution bake, the final sodium content must be homogeneous on a microscopic scale since a concentration gradient could not persist at the high temperatures reached during baking.

An upper bound on the inhomogeneity in the Na content is set by the width of the lines in x-ray powder patterns. According to the Brown-Banks relation mentioned above, any variation in the sodium content x would show up as a variation in the lattice constant. If we assume that the observed linewidth in our samples is due entirely to variations in the lattice constant, then x is constant throughout the samples to within about 0.015. This is almost certainly an overestimate, however, because the observed linewidth is near the limit of instrumental resolution. The sensitivity of the x-ray linewidths to variations in the Ta content is not sufficient to allow useful bounds to be set on the Ta inhomogeneity.

III. NMR INSTRUMENTATION

This section describes the experimental apparatus and procedures used for pulsed NMR measurements of the ^{183}W spin system in $Na_xTa_yW_{1-y}O_3$. Knight shift, absorption line shape, spin-lattice relaxation time T_1, and spin-spin phase memory time T_2 were measured in a field of 6.0 T at a temperature of 4.2 K. Some measurements were also made at 77 K.

^{183}W has spin $\frac{1}{2}$ and a natural abundance of 14.3%. The other naturally occurring isotopes of W all have spin zero. ^{183}W has one of the smallest magnetic moments of all spin-$\frac{1}{2}$ nuclei. Its moment is 0.115 nuclear magnetons, about $\frac{1}{24}$ of the moment of the proton. The small moment, along with a low natural abundance, makes tungsten NMR very difficult and places stringent requirements on our pulsed NMR spectrometer.

The 6.0-T field is produced by an Oxford Instruments superconducting magnet. At that field, the ^{183}W resonance occurs at 10.6 MHz. The field variation over the sample volume is about 0.050 G, and the field drift is less than 1 part in 10^7 per day. This excellent field stability is essential for our measurements of very long spin-lattice relaxation times—measurements which often required days of signal averaging.

Sample temperatures of 4.2 and 77 K are established by immersing the sample directly in liquid helium or liquid nitrogen.

Much of the NMR electronics used in this study came to us compliments of Clark. The transmitter, a venerable unit built by Clark while a graduate student, is a class-C, tuned rf amplifier which can deliver about 2 kW of output power during a pulse.[19,20] The tank circuit and associated matching circuits follow a design by Clark and McNeil.[21] The preamp is a broadband, low-noise, high-input impedance amplifier also designed and built by Clark.

Because the magnetic moment of tungsten is so small and because the tungsten linewidths in our bronze samples are so large (see Sec. IV), a very large rf field H_1 is required in order to keep the lengths of our $\pi/2$ pulses short compared to the spin-dephasing time T_2^*. Our Clark spectrometer produces an H_1 of about 240 G in the sample coils used in this experiment. During a pulse, the peak voltage across the tuning capacitor of the tank circuit is 6000 V. Because of the high voltage, the tuning capacitor, an air-core capacitor with a plate separation of 2.5 mm, had to be painted with several coats of a high-breakdown-voltage dielectric in order to prevent arcing.

Each NMR sample consists of 6 g of bronze powder mixed with 1 g of tungsten-metal powder and dispersed in a block of paraffin wax. The tungsten metal is used as a Knight-shift reference.[22] Dispersion in wax makes the samples nonconducting, ensuring good rf penetration and minimizing eddy-current losses in the tank circuit.

Because of the high power of the transmitter, ringdown noise lasting as long as 0.5 msec is seen by the receiver following a pulse, in spite of the fact that the sample coil is potted in 1266 Stycast (made by Emerson and Cuming, Inc.) to minimize magneto-acoustic ringing. The broad NMR lines of the samples, with T_2^*'s as short as 50 μsec, generate free-induction decays (FID's) which are always obscured by ringdown noise. For this reason all of the NMR measurements are made on spin echoes. For the bronzes, T_2 is typically 10 msec, and so it is possible to separate the spin echo from the last pulse by 1 or 2 msec without significant loss of signal.

Standard pulse sequences are used in the measurements of Knight shift, T_1, and T_2. For these measurements, signal averaging is required. This is accomplished with a Nicolet series 1170 signal-averaging system with a 1-MHz digitizer. Unfortunately, the Nicolet machine, like most digital electronics, produces so much rf noise that it cannot be connected directly to the NMR spectrometer without completely scrambling the tiny nuclear signal. To solve this problem, the trigger input of the Nicolet is isolated from the pulse generator of the NMR spectrometer by an opto-isolation switch, and the signal input of the Nicolet is isolated from the receiver by a unity gain instrumentation amplifier. With these buffers in place, signals can get into the Nicolet, but no noise can come out.

The absorption line shape is measured by the Clark method.[19] In the Clark method a boxcar integrator is used to perform an analog Fourier transform of the FID. Briefly said, the gate of the boxcar is set to cover the entire spin echo, and the integrated area of the echo is measured as the field is swept through resonance. The echo area versus field, or the equivalent frequency, is the absorption line shape.

IV. EXPERIMENTAL RESULTS

Figure 1 is a plot of the conductivity versus temperature for several different samples of $Na_xTa_yW_{1-y}O_3$. The location of Mott's minimum metallic conductivity[23] σ_{min} is indicated on the figure. The value of σ_{min} is calculated from the relation

$$\sigma_{min}=(0.025)e^2/\hbar a \ . \tag{1}$$

The mean distance between scattering centers, a, is taken to be

$$a=n_c^{-1/3} \ , \tag{2}$$

where n_c is the critical conduction-electron concentration.

The conductivity of the $x=0.34, y=0.16$ sample has a remarkable temperature dependence. Its conductivity is proportional to temperature over the whole range studied ($1.6<T<300$ K). In a previous paper,[24] we discussed these data in some detail and concluded that this sample has a composition which puts it very close to the M-I transition. (We should mention that although the conductivity of the $x=0.27, y=0.16$ sample appears to be approaching a nonzero value as $T\rightarrow 0$, we nevertheless regard this sample as an insulator since its low-temperature conductivity is at least 6 orders of magnitude below σ_{min}.)

Figure 2 shows the ^{183}W magnetization recovery curves at $T=4.2$ K in a field of 6.00 T for four Ta-doped samples that span the M-I transition. (NMR sample numbers and compositions are listed in Table I.) The amplitude of the spin echo, which is proportional to the nuclear magnetization, is plotted versus the time following a saturation comb which sets the nuclear magnetization to zero. The data have been scaled so that equilibrium magnetiza-

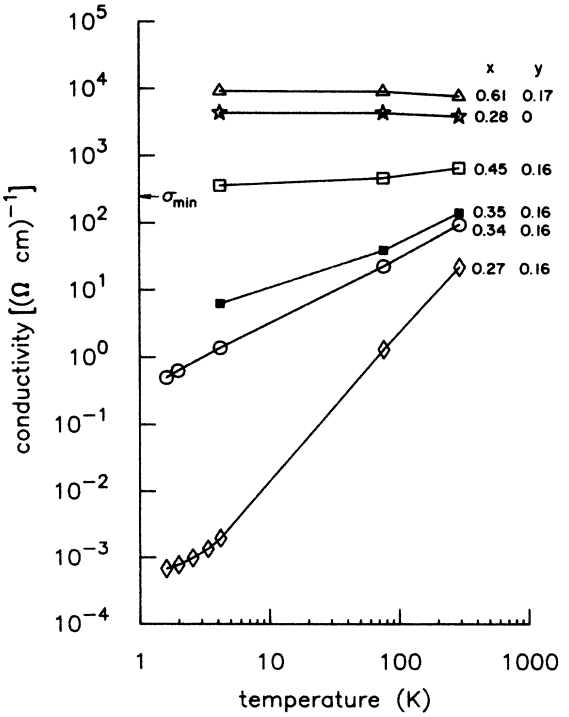

FIG. 1. dc conductivity vs temperature for several samples of $Na_xTa_yW_{1-y}O_3$.

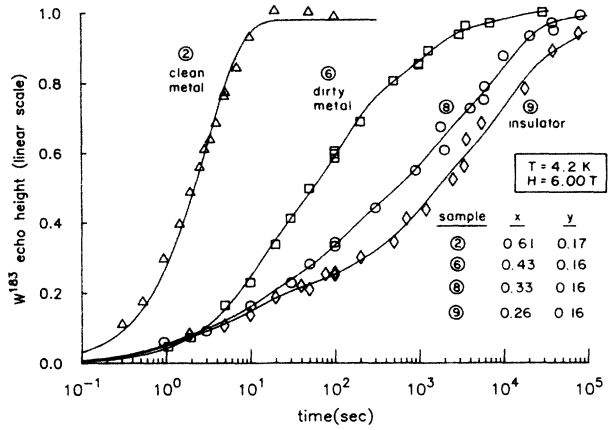

FIG. 2. ^{183}W magnetization recovery curves for four samples spanning the M-I transition. The lines through the data are fits to the expression for multiple relaxation-time recovery, Eq. (3).

tion corresponds to an echo height of 1.0.

Sample 2, a relatively good metal, shows nearly perfect exponential recovery. The solid curve drawn through the data for that sample is a pure exponential recovery curve with $T_1 = 3.0$ sec. The other samples cannot be characterized by single relaxation times because their recovery curves are nonexponential. That these curves are nonexponential can be seen from Fig. 3, which displays exponential recovery curves with four different time constants along with experimental data for sample 9, the insulator. One should note that on this linear-log plot all exponential curves have the same shape. They are simply translated along the time axis. By comparing the data for the insulating sample with the exponential curves, one can see that the insulating sample is properly described by a distribution of relaxation times.

In order to extract the distribution of relaxation times, the recovery curves for each sample were fitted to an equation of the form[25]

$$M(t) = \sum_{i=1}^{6} A_i (1 - e^{-t/T_i}) , \qquad (3)$$

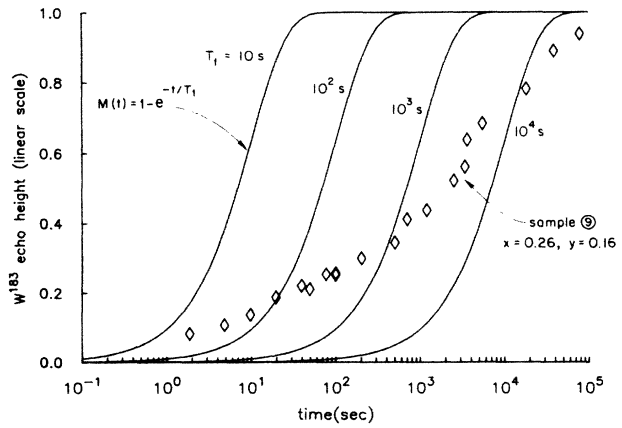

FIG. 3. Exponential magnetization recovery curves and data for the nonexponential recovery of the insulating sample (sample 9) at T=4.2 K.

where the T_i's are fixed at 1,10,100, . . . , 100 000 sec. The A_i's are the fitting parameters. A_i is interpreted as the fraction of the nuclei with relaxation times near T_i. The fits are plotted in Fig. 2 and the A_i's are displayed in Fig. 4. Also shown in Fig. 4 are the A_i's resulting from a fit to the recovery curve for sample 4 ($x = 0.26, y = 0$). For this sample an excellent fit resulted from fixing the T_i's in Eq. (3) at 1, 3, 10, 30, 100, and 300 sec. Estimated uncertainties in the A_i values lie in the range 0.02—0.04. These error estimates are confirmed by the reproducibility of the A_i values of samples 7 and 8, which have nearly the same composition (data for sample 7 not shown here).

From Fig. 4 we see that samples near the transition and on its insulating side are characterized by a wide distribution of spin-lattice relaxation times, with the distribution broadening and shifting toward longer times in the more insulating samples. In samples 8 and 9, the most insulating samples, approximately 10% of the nuclei relax in seconds—a relaxation-time characteristic of metallic environments—while the other nuclei relax in minutes or hours, characteristics of spin-$\frac{1}{2}$ nuclei in insulators.

We will argue in Sec. VI that the ^{183}W nuclei are completely uncoupled from one another, i.e., that there is no nuclear-spin diffusion. If this is the case, then each nucleus relaxes at a rate determined entirely by its immediate electronic environment, and the distribution of relaxa-

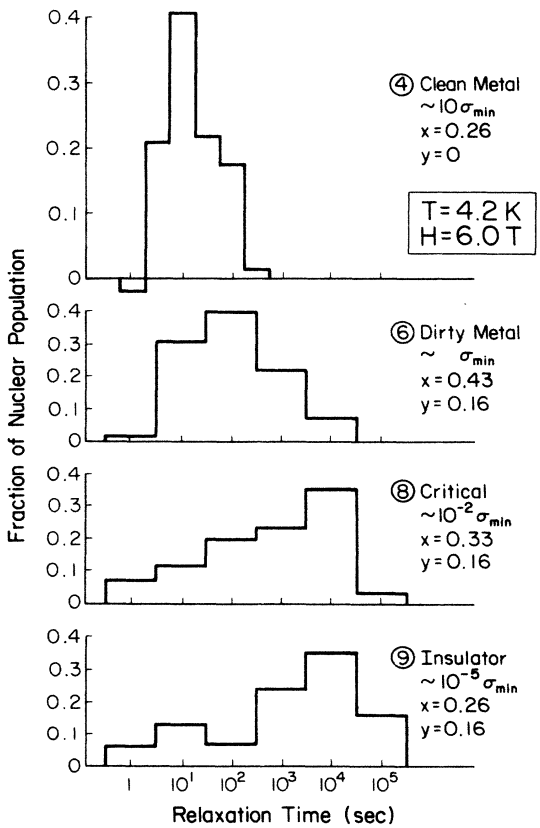

FIG. 4. Distribution of spin-lattice relaxation times resulting from fits of the data in Fig. 2 to Eq. (3). Note that the bin size on the time axis in the top plot (sample 4) is half of that in the lower plots. The A_i scale on the top plot (sample 4) has therefore been doubled so that all plots cover the same area.

tion times senses the distribution of local electronic environments.

Figure 5 displays the correlation between the conductivity and the distribution of relaxation rates. Both the Ta-doped and the undoped samples follow a common trend. As the conductivity is decreased through the *M-I* transition, the distribution of rates widens continuously. Note that the fastest-relaxing nuclei in all of the samples, both metallic and insulating, have T_1's of a few seconds. Also note that no sudden change in the distribution of local relaxation rates marks the *M-I* transition. This last property is characteristic of second-order phase transitions. Examined locally, the system evolves smoothly in the vicinity of the transition and gives no hint of the drastic conductivity changes occurring on a global scale.

Some T_1 measurements were made at $T=77$ K as well as at $T=4.2$ K. Figure 6 shows the magnetization recovery curves for sample 5 ($x=0.24, y=0$) at 4.2 and 77 K. Also plotted are the 77-K data artificially shifted to times that are longer by a factor of 77/4.2. We see from the coincidence of the shifted 77-K data and the 4.2-K data that each T_1 in the distribution of T_1's is proportional to $1/T$. In Fig. 7 we see the same behavior in sample 6 ($x=0.43, y=0.16$). Sample 6 is a dirty metal with a conductivity at or near $\sigma_{\min}$. The relation $T_1 \propto 1/T$ was derived by Korringa for the case of clean metals,[26] and it is perhaps surprising to see this relation obeyed in such a dirty system.

Table I lists peak Knight shifts, spin-lattice relaxation times T_1, and spin-spin phase memory times T_2 for the bronze samples. The peak Knight shift is the shift of the

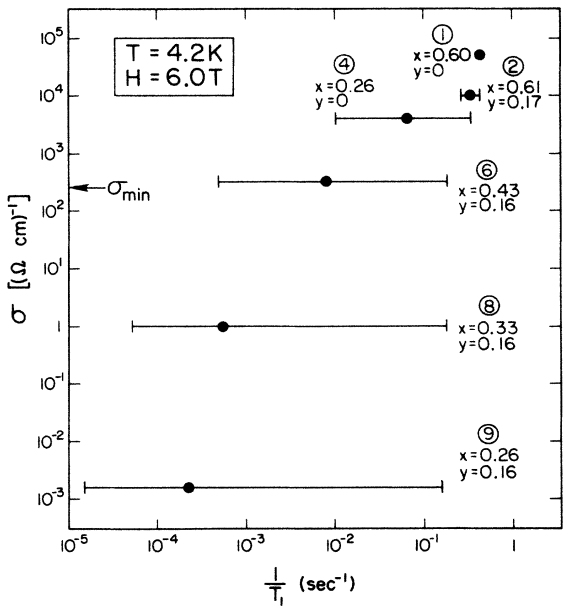

FIG. 5. Distribution of relaxation rates vs conductivity for several samples of $Na_xTa_yW_{1-y}O_3$. The solid circles indicate $1/T_1'$, where T_1' is the time required for the nuclear magnetization to reach $1-1/e$ of its equilibrium value. The bars give a measure of the width of the distribution of relaxation rates. About 20% of the nuclear population have relaxation rates outside the bounds marked by the bars. 10% have faster rates; 10% have slower rates.

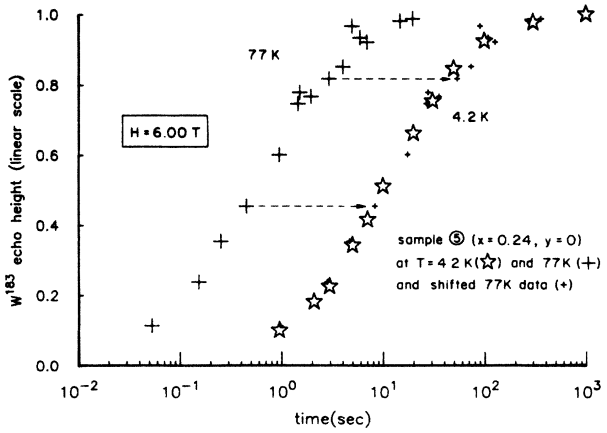

FIG. 6. Magnetization recovery curves for sample 5 ($\sigma \approx 10\sigma_{\min}$) at $T=4.2$ and 77 K. 77-K data are also shown artificially shifted to times that are longer by the factor 77/4.2.

peak of the absorption line. All samples exhibited inhomogeneously broadened lines and so are properly characterized by a distribution of shifts rather than a single shift (see Fig. 8). Monoclinic tungsten trioxide, WO_3, is taken as the Knight-shift reference. For samples 4—9, which exhibit nonexponential relaxation, T_1 is defined as the time required for the magnetization to reach $1-1/e$ of its equilibrium value.

Also listed in Table I are the spin-lattice relaxation times of the insulators, tungsten trioxide, WO_3, and sodium tungstate, Na_2WO_4. No signal was seen in the Na_2WO_4 sample even after it was allowed to relax in a field of 6.0 T at $T=4.2$ K for 16 h. This null result sets a lower limit of 160 h for the T_1 of ^{183}W in sodium tungstate. In WO_3, no signal was seen after 1 h of relaxing, but a weak signal was seen after 18 h. On the basis of this single data point, we calculate a T_1 of 60 ± 10 h in WO_3. Note that these times, 160 and 60 h, are longer than the time required for full relaxation of the most insulating bronze samples (~ 24 h).

We have computed T_2 for ^{183}W in the bronzes due to W-Na and W-Ta nuclear-dipole—dipole coupling[8] and

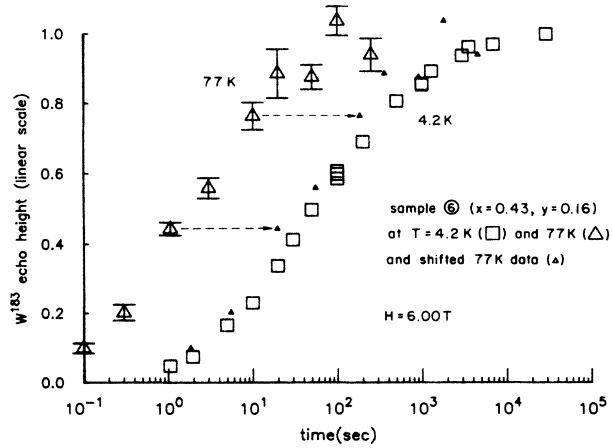

FIG. 7. Magnetization recovery curves for sample 6 ($\sigma \simeq \sigma_{\min}$) at $T=4.2$ and 77 K. As in Fig. 6, 77-K data are also shown shifted to times that are longer by the factor 77/4.2.

TABLE I. NMR properties of $Na_xTa_yW_{1-y}O_3$.

Sample	x	y	T (K)	K(WO_3)	T_1 (sec)	T_2 (msec)
1	0.60	0	4.2	−0.23(2)%	2.32±0.07	
2	0.61	0.17	4.2	−0.19(1)%	3.0 ±0.1	
3	0.60	0.16	4.2	−0.20(2)%	3.5 ±0.2	
4	0.26	0	4.2	−0.086(5)%	16[a]	
5	0.24	0	4.2	−0.045(5)%	17	14.2±0.4
			77	−0.100(2)%		
6	0.43	0.16	4.2	+0.012(5)%	127	
			77	−0.004(5)%		
7	0.32	0.16	4.2	+0.016(1)%	1870	
8	0.33	0.16	4.2	+0.014(5)%	1740	9.0±0.4
9	0.26	0.16	4.2	+0.012(2)%	4920	8.4±0.4
WO_3				0	60 ±10 h	
Na_2WO_4				?	> 150 h	

[a]Samples 4—9 exhibit nonexponential relaxation. For these, T_1 is defined as the time required for the magnetization to reach $1-1/e$ of its equilibrium value.

find good agreement with the measured values listed in Table I. The contribution to T_2 from W-W nuclear-dipole coupling is negligible.

In Fig. 8 are displayed the peak Knight shifts and full linewidths at half maximum (FWHM) for selected samples. The metallic samples exhibit very wide, inhomogeneously broadened lines with overall negative Knight shifts. Our results for metallic samples are consistent with those of Weinberger's NMR study[13] of metallic Na_xWO_3. The negative Knight shift indicates that core polarization is the principal mechanism contributing to the shift.[27] The wide line is caused by a distribution of Knight shifts corresponding to a distribution of local electronic environments in these disordered materials. As we move through the *M-I* transition, the peak Knight shift falls to nearly zero, and the distribution of shifts collapses around that zero.

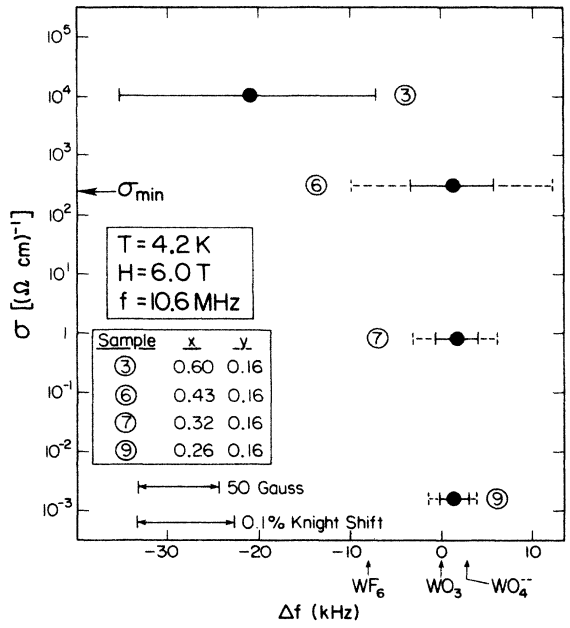

FIG. 8. ^{183}W Knight-shift spread vs conductivity in $Na_xTa_yW_{1-y}O_3$. Solid circles indicate the position of the peak of absorption line. The dashed lines give the FWHM linewidths of the "fast relaxers," those with T_1's ≤ 30 sec. The solid lines give the FWHM linewidths of the full nuclear population, both slow and fast relaxers.

The linewidths for the more insulating samples, those with a distribution of relaxation times, are difficult to characterize because nuclei with different relaxation times were found to have different line shapes. Those nuclei that relaxed quickly (seconds) had a broader line shape; those that relaxed slowly (hours) had a narrower line. Two linewidths are shown in Fig. 8 for each of the more insulating samples. The larger linewidth (shown by a dashed line) is that of the "fast relaxers" (those nuclei that relax within about 30 sec) and is measured by the Clark technique described in Sec. III (Ref. 28). The smaller linewidth (shown by a solid line) is that of all the spins (slow as well as fast relaxers) and was determined from the spin-echo shape at long times.

V. REVIEW OF ELECTRON-NUCLEUS COUPLING MECHANISMS

In preparation for a discussion of the NMR results that were presented in Sec. IV, we list the different interactions which couple electrons to spin-$\frac{1}{2}$ nuclei in solids and which are responsible for the Knight shift and the spin-lattice relaxation rate in metals. Among the most important mechanisms are the following:

(a) The contact interaction with unpaired electrons at the Fermi surface.

(b) Core polarization, the contact interaction with closed-shell electrons which have a nonvanishing spin density at the nucleus as a result of an exchange interaction with polarized electrons at the Fermi level.

(c) The orbital interaction between the nuclear moment and the orbital moment of electrons in partly filled shells.

(d) The nuclear-spin—electronic-spin dipolar interaction.

There are at least two other possible spin-lattice relaxation mechanisms: spin diffusion to paramagnetic impurities and coupling to nuclei of another species. In clean metals, the relaxation rates due to these mechanisms are negligibly small, but because we will be considering extremely long T_1's in samples near the M-I transition, we cannot ignore any mechanism. In Sec. VI we will argue that impurity relaxation is negligible in our samples. With regard to coupling to other nuclear species, we have estimated the ^{183}W spin-lattice relaxation rate due to ^{183}W-^{23}Na dipole coupling in Na_xWO_3 (Ref. 8) and find that it is smaller than 10^{-7} sec^{-1}. This rate is 2 orders of magnitude smaller than the smallest rate seen in any of our samples and thus small enough to be negligible. The ^{183}W-^{181}Ta coupling is expected to yield a comparable relaxation rate and so can also be safely ignored. Coupling to ^{17}O, the only naturally occurring isotope of oxygen with nonzero spin, is negligible because of its low natural abundance (0.04%).

The contact interaction is usually the dominant coupling mechanism in metals of low atomic number. If the nearly-free-electron approximation is valid, the contact-interaction-induced Knight shift K_s and spin-lattice relaxation time T_{1s} obey the Korringa relation[26]

$$K_s^2 T_{1s} T = (\gamma_e/\gamma_n)^2 \hbar/4\pi k = \delta \ . \tag{4}$$

T is the temperature, γ_e and γ_n are the electronic and nuclear gyromagnetic ratios, respectively, and k is Boltzmann's constant. δ is called the Korringa constant.

The core-polarization (CP) interaction is often important in d-band metals and causes a Knight shift K_d that is negative; i.e., the induced local field subtracts from the external field.

Using band theory, Yafet and Jaccarino[27] showed that the CP-induced Knight shift K_d and spin-lattice relaxation time T_{1d} obey a Korringa-like relation

$$K_d^2 T_{1d} T = \delta/q \ , \tag{5}$$

where δ is the Korringa constant and q is a parameter which lies between $\frac{1}{5}$ and $\frac{1}{2}$ and depends on the proportion of t_{2g} d orbitals in the electronic wave functions at the Fermi surface. For a metal whose conduction band is made up primarily of t_{2g} orbitals, q is near $\frac{1}{3}$. According to band-structure calculations,[29,30] Na_xWO_3 is such a metal.

The orbital interaction produces a Knight shift $K_{\rm orb}$ and a spin-lattice relaxation time $T_{1,\rm orb}$ in p- and d-band metals.[31] Because the orbital Knight shift is a second-order effect, no Korringa-like relation analogous to Eqs. (4) and (5) holds for the orbital interaction.

The dipole interaction produces no shift in metals of cubic symmetry and an anisotropic shift in metals of lower symmetry.[32] The spin-lattice relaxation rate due to the dipole interaction can be expressed as a fraction of the rate due to the orbital interaction.[31] For d-band metals the fraction is about 0.1. We will assume that the dipolar interaction is negligible in the bronzes.

In the transition metals, contact, core-polarization, and orbital interactions can all contribute significantly to the total Knight shift and spin-lattice relaxation rate. The total relaxation rate and shift can be written

$$1/T_1 = (1/T_1)_s + (1/T_1)_d + (1/T_1)_{\rm orb} \ , \tag{6}$$

$$K = K_s + K_d + K_{\rm orb} \ . \tag{7}$$

Note that the rates always add, but that the shifts can cancel because the core-polarization shift is negative.

The contributions of the different rates depend on the relative size of $\rho_s(E_F)$ and $\rho_d(E_F)$, the s- and d-orbital contributions to the density of states at the Fermi level. In general,[33] $(1/T_1)_s \propto T\rho_s^2(E_F)$ and $(1/T_1)_d, (1/T_1)_{\rm orb} \propto T\rho_d^2(E_F)$. The nuclei are relaxed through spin-flip collisions with conduction electrons. However, because an electronic moment is so much larger than a nuclear moment, simply flipping spins in the external field will not conserve energy. The electron must have an empty electronic state nearby in energy to scatter into in order to take up the energy difference. Only states within kT of the Fermi surface have such empty states available. For this reason, none of these mechanisms can relax spin-$\frac{1}{2}$ nuclei in band-gap insulators. In such systems the dominant relaxation process is usually spin diffusion to paramagnetic impurities.[34] If the material is very pure, T_1 can be unmeasurably long—days or months.

VI. DISCUSSION OF RESULTS

A. NMR properties of the metallic bronzes

We begin our discussion of the interpretation of the NMR results by considering samples with high values of $x-y$. In these good metallic samples, we expect the formulas in Sec. V, developed within the approximations of band theory, to be valid. The peak Knight shifts in these samples are negative. Evidently, core polarization makes the dominant contribution to the shift. We might hope that core polarization also dominates the relaxation rate. Band-structure calculations[29] for $NaWO_3$ indicate that the conduction band is made up almost entirely of tungsten $5d(t_{2g})$ and oxygen $2p$ orbitals, with very little tungsten $6s$ character, and so we have some reason to expect that the contact interaction is small. If CP is the only mechanism at work, then Eq. (5), the CP Korringa relation, is valid. Taking $q=\frac{1}{3}$, as the band-structure calculations indicate, Eq. (5) yields

$$(K^2 T_1 T)_{\rm CP} = 4.6\times 10^{-4} \ \text{sec K} \ .$$

Table II lists Korringa products, K^2T_1T, for each of four metallic samples. In these samples, the peak Knight shift varies from -0.25% to -0.19% and T_1 (at 4.2 K) varies from 1.6 to 3.0 sec, yet the Korringa product is

TABLE II. Values of K^2T_1T for some metallic samples of $Na_xTa_yW_{1-y}O_3$. Data for the first two samples shown are from Weinberger's work (Ref. 13).

x	y	K^2T_1T (10^{-5} sec K)
0.84	0	4.7±0.5
0.74	0	5.2±0.8
0.60	0	5.1±1.0
0.61	0.17	4.6±0.6

constant within experimental errors and equal to about 5×10^{-5} sec K.

The experimental value of K^2T_1T is a factor of 10 smaller than the theoretical value obtained by assuming that CP is the only coupling mechanism. This discrepancy could be due to a contact interaction, either with W 6*s* or O 2*p* orbitals. The band-structure calculations indicate that O 2*p* is the more likely suspect.

Narath gives a Korringa-like relation between the total shift and relaxation rate when the contact and CP interactions are the only coupling mechanisms present.[33] If we can ignore the orbital interaction, Narath's formula allows us to compute the relative contributions of contact and CP interactions to the total shift and relaxation rate. The results are[8]

$$K_d/K_s=-1.8,\quad (1/T_1)_d/(1/T_1)_s=1.1\ .$$

(Following a common convention, the subscript *s* refers to the contact interaction even though the interaction may, in this case, arise from the O 2*p* orbitals.)

If the orbital interaction was significant in the bronzes, then we would not expect K^2T_1T to be a constant. This is because, as mentioned in Sec. V, the orbital shift and relaxation rate do not obey a Korringa relation.

We conclude that the contact and core-polarization interactions are the dominant electron-nucleus coupling mechanisms in the metallic sodium tungsten bronzes. Orbital and dipolar interactions are insignificant. The CP Knight shift is about twice the contact shift, and the contributions of the two mechanisms to the total relaxation rate are about equal.

The line shapes for three metallic samples (all with $\sigma\gg\sigma_{\min}$) are shown in Fig. 9. As mentioned in Sec. IV, the wide, inhomogeneously broadened lines are due to a distribution of local Knight shifts arising from a distribution of local electronic environments. We would like to know what feature of the local electronic environment determines the shift. Sundfors and Holcomb,[35] in considering doped Si, argued that the local conduction-electron concentration n_e determines the local shift. In the case of $Na_xTa_yW_{1-y}O_3$, we are faced with the problem of computing n_e given the (presumably random) local configuration of sodium donors and tantalum acceptors. The problem is further complicated by the presence of two Knight-shift contributions of competing sign. We will simply ignore this last complication and assume that the Knight shift K is negative and that $K\propto n_e$. The fact that the transition occurs near $x=0.2$ in Na_xWO_3 (which is approximately the value for first-nearest-neighbor percolation) indicates that the local physics is dominated by nearest-neighbor (NN) interactions.[36] Therefore, we suggest, as a crude first approximation, that n_e and K at a particular tungsten site are proportional to the number of first-NN sodium atoms minus the number of first-NN tantalum atoms (NN Na's − NN Ta's). In Fig. 9 we plot the probability distribution of NN Na's − NN Ta's for the three samples whose measured line shapes are shown. The distributions, which are normalized to unit peak height for ease of comparison, are computed assuming random, uncorrelated placement of sodium and tantalum atoms.

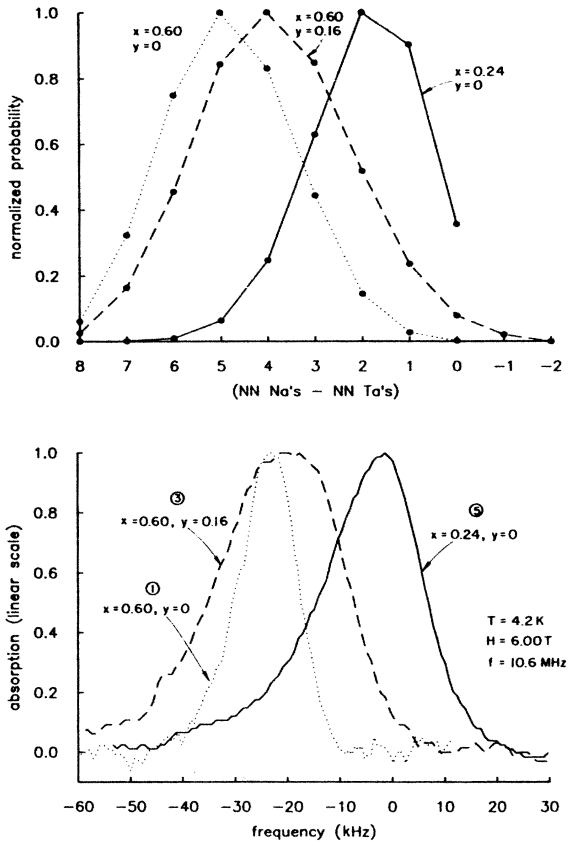

FIG. 9. Normalized probability distributions of number of nearest neighbors in $Na_xTa_yW_{1-y}O_3$ (see text) for three different compositions (top) and measured line shapes for samples with the same three compositions (bottom).

We see a qualitative similarity between the two plots. (But note well that the origin and the scale of the x axes have been adjusted for best comparison.) The asymmetry in the measured line shape of the $(x=0.24, y=0)$ sample appears in the model. The model also correctly predicts the relative positions of the peak Knight shifts in the $(x=0.60, y=0)$ and $(x=0.60, y=0.16)$ samples. However, the predicted linewidth of the undoped sample is too large compared to that of the tantalum-doped sample. Also, by design, the model cannot explain the positive Knight shifts seen in parts of the $(x=0.24, y=0)$ line. The positive and negative Knight shifts in the $(x=0.24, y=0)$ sample as well as in more insulating samples (see Fig. 8) arise from the competition between the contact and core-polarization interactions. Evidently, in the more insulating samples the local wave-function character fluctuations from site to site in the lattice—here more *s*-like with a positive shift and there more *d*-like with a resulting negative shift.

The great increase in the linewidth of a metallic bronze upon addition of tantalum can be understood qualitatively in the following terms. A tantalum atom in the bronze matrix has a net charge of $-e$ (it is an acceptor). Friedel oscillations in the electronic charge density appear around the tantalum site as the conduction electrons attempt to screen out the charged impurity. This variation in the total conduction-electron charge density leads to a variation

in the local Knight shift. This mechanism has been invoked to explain the broad Knight-shift distributions that are seen in a variety of alloys.[37]

B. NMR properties of the barely metallic and insulating bronzes

An unusual feature of the NMR properties of the bronzes is the appearance of dramatically nonexponential spin-lattice relaxation in the more insulating samples. In most systems of spin-$\frac{1}{2}$ nuclei in solids, the nuclei exchange energy among themselves (through dipole-dipole coupling, etc.) faster than they give up energy to the lattice. In such a case, the spin system remains in rough internal thermal equilibrium (with a well-defined spin temperature distinct from the lattice temperature), and the nuclear magnetization relaxes exponentially.

We now argue that, in contrast to the usual situation just described, ^{183}W spin diffusion does not occur in $Na_xTa_yW_{1-y}O_3$, at least not in the more insulating samples. In the tungsten bronzes the combination of the extremely small moment of ^{183}W and a wide spread in local fields kills spin diffusion and makes establishment of a spin temperature impossible. Each nucleus relaxes at a rate determined by its immediate electronic environment. There is no single time constant for the whole spin system, and nonexponential relaxation is the result.

There are at least two internucleus coupling mechanisms which can produce nuclear spin diffusion: the direct dipole-dipole interaction and the Ruderman-Kittel interaction, an indirect exchange coupling between nuclei mediated by conduction electrons.[38] In order for spin diffusion to occur, the dipole- or exchange-field-coupling nearest-neighbor nuclei must be greater than any variation in the local fields at the two nuclei—a variation due to, say, an inhomogeneous external field or a distribution of local Knight shifts. If this condition is not satisfied, energy-conserving mutual spin flips cannot occur, and spin diffusion is inhibited. For the bronzes, the distribution of local Knight shifts indicates a huge spread in the local fields—hundreds of gauss in the metallic samples and 20 or 30 G in the most insulating sample. Compared to this large inhomogeneous linewidth, the dipole field due to a nearest-neighbor ^{183}W nucleus is minuscule ($\approx$0.01 G).

The magnitude of the exchange field in metals is difficult to estimate, but it is often larger than the dipole field. For example, Dubson[39] measured the strength of the exchange interaction which couples nearest-neighbor ^{183}W nuclei in W metal and found it to be about 5 times larger than the strength of the dipole coupling. Even though the exchange field in the bronzes may be much larger than the dipole field, it is certainly not as large as the linewidth. In any case, the exchange coupling only exists in the metallic samples; it vanishes in the insulating samples. Since the coupling is mediated by conduction electrons, as soon as the electron mean free path is less than a lattice constant (this occurs when $\sigma < \sigma_{\min}$), the coupling fades away.

Our argument implies that spin diffusion is inhibited in both insulating and metallic bronzes. However, samples with $\sigma \gg \sigma_{\min}$ exhibit near-prefect exponential relaxation [for example, sample 2 ($x=0.60, y=0.16$)]. Either our argument breaks down for the metal samples (through the appearance of a spin-coupling mechanism not included in our simple picture) or the uncoupled nuclei all relax at the same rate, a situation in apparent conflict with the spread in hyperfine coupling strengths indicated by the broad Knight-shift distribution.

We can reject two alternate interpretations of the nonexponential recovery curves. The first interpretation is that our samples contain magnetic impurities, such as iron. Slow spin diffusion to paramagnetic impurities might result in nonexponential relaxation.[34] However, T_1 measurements in the insulators WO_3 and Na_2WO_4 (see Table I) indicate that our samples are clean. Any trace impurities in the bronze samples probably came from the starting materials, WO_3 and Na_2WO_4. (The Ta_2O_5 used in the bronze manufacture was of much higher purity than the tungsten compounds.) Since impurity relaxation is exceedingly slow in the starting materials, it seems safe to assume that it is not the dominant relaxation mechanism in the product.

A second possible interpretation of the nonexponential behavior is that our samples are grossly inhomogeneous. Suppose that the bronze samples were so inhomogeneous that the Na (or Ta) atoms formed large, dense clumps, micrometers in size, separated by large Na- (or Ta-) poor regions. One could then regard the samples as consisting of small metallic grains dispersed by insulating grains. In that case, the observed distribution of relaxation times has a simple explanation. The fast-relaxing nuclei are the ones in the metallic grains, and the slow relaxers are in the insulating grains. However, this clumping model is inconsistent with both the narrow x-ray linewidths seen in our samples[40] and the narrow NMR linewidths of the insulating samples shown in Fig. 8. If the insulating samples were granular, then we would see a very broad NMR line, with the metallic environments producing the large Knight shifts seen in the metal samples and the insulating environments producing much smaller shifts.

To reiterate, since no spin diffusion occurs in this system, the distribution of relaxation rates senses the distribution of local electronic environments. In some sense, the fast relaxers are in metal-like locales, while the slow relaxers see insulating environments.

We would like to have a model which connects the local relaxation rate to some feature of the local electronic structure. Unfortunately, there exists no general theory of NMR in solids near a *M-I* transition. In the absence of a comprehensive model, we compare our results with the predictions of the standard Korringa model, which is strictly valid only for clean metals, and the Warren-Gotze-Ketterle model[41,42] of enhanced relaxation in dirty metals. Both of these models assume the existence of a spin temperature and single relaxation rate.

We begin by noting a qualitative similarity between our results and the behavior predicted by the Korringa model, Eq. (4). In sample 6, which has a conductivity near Mott's $\sigma_{\min}$, we find T_1 proportional to $1/T$ for each T_1 in the distribution of T_1's. From Fig. 8 we see that the more insulating samples with the longer relaxation times possess narrower distributions of Knight shifts. And

within each sample, the fast relaxers have the broader distribution of Knight shifts, while the slow relaxers have a narrower spread in shifts. We see a correlation between the small shifts and long relaxation times just as in the Korringa formula. A more detailed comparison with the Korringa model is inhibited by the presence of at least two electron-nucleus coupling mechanisms, core polarization and the contact interaction.

It is tempting to conclude that some kind of local Korringa relation is at work, that the local relaxation rate is given by $1/T_1 \propto \rho^2_{\text{local}}(E_F)$, where ρ_{local} is a local density of states, the density of those states that have appreciable wave-function overlap with the nucleus. The notion of a local Korringa relation in samples near a *M-I* transition is not without precedent. Very similar behavior (nonexponential relaxation with the spread in T_1's correlated to the spread in shifts) has been seen in doped silicon and interpreted in the same way.[43–45]

Unfortunately, we have not been able to test one important prediction of the Korringa model, the field independence of the Korringa product K^2T_1T. We have data only at $H=6$ T and $T>4.2$ K. At lower fields, poor signal-to-noise ratios make measurements impossible with our present apparatus.

Paalenen *et al.*[46] found a strong field dependence in the relaxation rate of ^{29}Si in doped Si at millikelvin temperatures near the *M-I* transition. Their results underscore the need for field-dependence data to completely characterize the spin dynamics in our system.

The suggestion that electron-nucleus spin-flip collisions remain the dominant nuclear relaxation mechanism on both sides of the *M-I* transition seems in conflict with the picture of disorder-induced localization of electronic states. Once the electronic eigenstates are localized, each nucleus sees a discrete spectrum of states. One might expect this to drastically inhibit nuclear relaxation since empty states at the Fermi level are needed in order for energy-conserving spin-flip collisions to occur. Using a density of states derived from Zumsteg's[47] specific-heat measurements in Na_xWO_3, we estimate an energy-level spacing of about 20 meV for a region containing 100 atomic cells. The electron spin-flip energy $2\mu_B H$ is only 0.7 meV at $H=6.0$ T. Thus, the conditions seem ripe for inhibition of the nuclear relaxation rate as a result of unavailable energy states. However, NMR studies of small platinum particles (in which the localization length is clearly the particle size) indicate no such inhibition of the relaxation rate.[48,49] So far as we know, the reason for this behavior is not certainly known. Perhaps lifetime broadening of the electronic levels produces the necessary quasicontinuum.

Warren[41] and Gotze and Ketterle[42] have developed a model for nuclear relaxation in dirty metals. The model assumes the existence of a spin temperature and that the contact interaction is the dominant electron-nucleus coupling mechanism. The model predicts that as σ is reduced below σ_{min} and electron motion becomes diffusive, the spin-lattice relaxation rate increases over the rate calculated from the Korringa relation [Eq. (4)] using the measured Knight shift. Roughly speaking, when electron motion is diffusive, electrons linger near nuclei and the spectral component of the fluctuating hyperfine field at the Larmor frequency increases, leading to an enhanced relaxation rate.

Because there at least two Knight-shift contributions of competing sign in the bronzes, the simple Korringa relation is not valid, and we cannot test the Warren-Gotze-Ketterle model directly. We do not see any clear indication of enhanced relaxation near the *M-I* transition. Note, however, from Figs. 4, 5, and 8, that the fast relaxers in the insulating samples have much smaller Knight shifts than the nuclei in the metal samples, and yet both have relaxation times of a few seconds. If spin diffusion did occur in this system, the fast relaxers in the insulators might relax the whole nuclear population in seconds, and one would see a considerable enhancement of the rate over that expected on the basis of the smaller Knight shift.

We conclude this section by noting that the Knight-shift data in Fig. 8 and Table I offer no evidence for the formation of local electronic moments on the insulating side of the transition. Sufficiently far into the insulating side, we expect to find a dilute system of isolated donor sites which exhibit a Curie-law susceptibility. In a field of 6.0 T at 4.2 K, the electronic moments of such donor sites would be nearly fully polarized. A population of moments of size μ and concentration c would produce a mean internal field of size $4\pi c\mu$, leading to a shift in the peak position of the NMR line toward higher frequencies. However, as we move through the transition from metal to insulator, the linewidth narrows continuously while the peak of the line remains constant (compare samples 6–9). We conclude that in our most insulating sample (sample 9) less than one sodium atom in 100 has a moment.

VII. CONCLUSIONS

To summarize, we have studied the NMR properties of the ^{183}W spin system in $Na_xTa_yW_{1-y}O_3$ on both sides of the *M-I* transition. In contrast to the dc conductivity, which changes dramatically at the *M-I* transition, the NMR properties evolve smoothly through the transition. Nuclear-spin diffusion is inhibited in this system by the combination of a large distribution of Knight shifts and a small nuclear moment. Consequently, no spin temperature is established, and NMR measurements provide a truly local probe of the electronic environment. In weakly conducting and insulating samples, we find a broad distribution of local spin-lattice relaxation rates. In moving through the transition from metal to insulator, the distribution of T_1's broadens and shifts toward longer times, while the distribution of Knight shifts narrows about a mean value that falls to near zero. Despite a complete breakdown of the nearly-free-electron approximation, the NMR properties of samples near the transition continue to display Korringa-like behavior. In samples with $\sigma \geq \sigma_{\text{min}}$, the relation $T_1 \propto 1/T$ is found to hold for each T_1 in the distribution of T_1's. And in all samples, there is a correlation between large Knight shifts and large spin-lattice relaxation rates. In the strong-scattering regime, we find no clear indication of an enhancement of the relaxation rate of the type described by Warren[41] and Gotze and Ketterle.[42] Finally, we see no evidence of

local-moment formation on the insulator side of the transition.

ACKNOWLEDGMENTS

We thank W. G. Clark for his electronics expertise. We are grateful to R. M. Cotts and N. W. Ashcroft for valuable discussions. This work was supported by the Cornell University Materials Science Center through National Science Foundation Grant No. DMR-82-17227-A01.

*Present address: Department of Physics, The Ohio State University, Columbus, OH 43210-1106.

[1]H. R. Shanks, P. H. Sidles, and G. C. Danielson, in *Non-Stoichiometric Compounds,* Vol. 39 of *Advances in Chemistry Series,* edited by Robert F. Gould (American Chemical Society, Washington, D.C., 1963), p. 237.

[2]P. A. Lightsey, D. A. Lilienfeld, and D. F. Holcomb, Phys. Rev. B **14**, 4730 (1976), and references therein.

[3]A. S. Ribnick, B. Post, and E. Banks, *Nonstoichiometric Compounds,* Vol. 39 of *Advances in Chemistry Series,* edited by Robert F. Gould (American Chemical Society, Washington, D.C., 1963), p. 246.

[4]The so-called cubic phase, stable for $x > 0.2$, actually undergoes a series of slight distortions from the perovskite structure as temperature and sodium content are varied. For this reason, the high-x bronze is sometimes referred to as pseudocubic. See, for instance, G. Bonera, F. Borsa, M. L. Crippa, and A. Rigamonti, Phys. Rev. B **4**, 52 (1971); R. Clarke, Phys. Rev. Lett. **39**, 1550 (1971).

[5]T. Wolfram and L. Sutcu, Phys. Rev. B **31**, 7680 (1984), and references therein.

[6]J. Doumerc, J. Marcus, M. Pouchard, and P. Hagenmuller, Mater. Res. Bull. **14**, 201 (1979).

[7]J. Doumerc, P. Dordor, E. Marquestaut, M. Pouchard, and P. Hagenmuller, Philos. Mag. B **42**, 487 (1980).

[8]M. A. Dubson, Ph.D. thesis, Cornell University, 1984 (unpublished).

[9]V. H. Jones, E. A. Garbaty, and R. G. Barnes, J. Chem. Phys. **36**, 494 (1962).

[10]A. Narath and A. T. Fromhold, Jr., Phys. Rev. **139**, A794 (1965).

[11]A. T. Fromhold and A. Narath, Phys. Rev. **136**, A487 (1964); **152**, 585 (1966).

[12]D. P. Tunstall, Phys. Rev. B **11**, 2821 (1975).

[12]B. R. Weinberger, Phys. Rev. B **11**, 2821 (1975).

[14]D. P. Tunstall and W. Ramage, J. Phys. C **13**, 725 (1980).

[15]H. R. Shanks, J. Crys. Growth **13-14**, 433 (1972).

[16]W. McNeill and L. E. Conroy, J. Chem. Phys. **36**, 87 (1962).

[17]P. F. Weller, B. E. Taylor, and R. L. Mohler, Mater. Res. Bull. **5**, 465 (1970).

[18]B. W. Brown and E. Banks, J. Am. Chem. Soc. **76**, 963 (1954).

[19]W. G. Clark, Rev. Sci. Instrum. **35**, 316 (1964).

[20]W. G. Clark, Ph.D. thesis, Cornell University, 1981 (unpublished).

[21]W. G. Clark and J. A. McNeil, Rev. Sci. Instrum. **44**, 844 (1973).

[22]The values of the Knight shift K reported in Sec. IV are with respect to WO_3. The calculation of K with respect to WO_3 from measurements of K with respect to tungsten metal involves a small correction for the temperature dependence of K of tungsten metal. See Ref. 8.

[23]N. F. Mott and E. A. Davis, *Electronic Processes in Non-Crystalline Materials,* 2nd ed. (Oxford University Press, New York, 1979), Chap. 2.

[24]M. A. Dubson and D. F. Holcomb, Phys. Rev. B **32**, 1955 (1985).

[25]A more sophisticated treatment of the data in Fig. 2 (for example, by Laplace-transform techniques) is inappropriate due to the limited quantity of data.

[26]C. P. Slichter, *Principles of Magnetic Resonance,* 2nd ed. (Springer-Verlag, Berlin, 1978), Chap. 5.

[27]Y. Yafet and V. Jaccarino, Phys. Rev. **133**, A1630 (1964).

[28]The Clark technique involves pulsing the system periodically while sweeping the field through resonance. The samples were pulsed once every 10—30 sec so that only those nuclei that relax within that short time are sampled.

[29]L. Koop, B. N. Harmon, and S. H. Liu, Solid State Commun. **22**, 677 (1977).

[30]D. W. Bullett, Solid State Commun. **46**, 575 (1983).

[31]Y. Obata, J. Phys. Soc. Jpn. **18**, 1020 (1963).

[32]A. Abragam, *The Principles of Nuclear Magnetism* (Oxford University Press, New York, 1961), pp. 199ff.

[33]A. Narath, *Hyperfine Interactions,* edited by A. J. Freeman and R. B. Frankel (Academic, New York, 1967), Chap. 7.

[34]*The Principles of Nuclear Magnetism,* Ref. 32, pp. 381ff.

[35]R. K. Sundfors and D. F. Holcomb, Phys. Rev. **136**, A810 (1964).

[36]P. A. Lightsey, Phys. Rev. B **8**, 3586 (1973).

[37]A. E. Blandin, E. Daniel, and J. Friedel, Philos. Mag. **4**, 180 (1959).

[38]M. A. Ruderman and C. Kittel, Phys. Rev. **96**, 99 (1954).

[39]M. A. Dubson, Phys. Rev. B **32**, 3485 (1985).

[40]C. P. Tunstall, Phys. Rev. B **10**, 4735 (1976).

[41]W. W. Warren, Jr., Phys. Rev. B **3**, 3708 (1971).

[42]W. Gotze and W. Ketterle, Z. Phys. B **54**, 49 (1983).

[43]D. Jerome, C. Ryter, and J. M. Winter, Physica **2**, 81 (1965).

[44]S. Kobayashi, Y. Fukagawa, S. Ikehata, and W. Sasaki, J. Phys. Soc. Jpn. **45**, 1276 (1978).

[45]M. J. Hirsch and D. F. Holcomb, Phys. Rev. B **33**, 2520 (1986).

[46]M. A. Paalanen, A. E. Ruckenstein, and G. A. Thomas, Phys. Rev. Lett. **54**, 1295 (1985).

[47]F. C. Zumsteg, Phys. Rev. B **14**, 1406 (1976).

[48]I. Yu, A. A. V. Gibson, E. R. Hunt, and W. P. Halperin, Phys. Rev. Lett. **44**, 348 (1980).

[49]H. E. Rhodes, P. K. Wang, C. D. Makowka, S. L. Rudaz, H. T. Stokes, and C. P. Slichter, Phys. Rev. B **26**, 3569 (1982).